Check for updates

ADVANCED MATERIALS
www.advmat.de

Unusual Temperature Dependence of Water Sorption in Semicrystalline Hydrogels

Xinyue Liu, Lenan Zhang, Bachir El Fil, Carlos D. Díaz-Marín, Yang Zhong, Xiangyu Li, Shaoting Lin, and Evelyn N. Wang**

Water vapor sorption is a ubiquitous phenomenon in nature and plays an important role in various applications, including humidity regulation, energy storage, thermal management, and water harvesting. In particular, capturing moisture at elevated temperatures is highly desirable to prevent dehydration and to enlarge the tunability of water uptake. However, owing to the thermodynamic limit of conventional materials, sorbents inevitably tend to capture less water vapor at higher temperatures, impeding their broad applications. Here, an inverse temperature dependence of water sorption in poly(ethylene glycol) (PEG) hydrogels, where their water uptake can be doubled with increasing temperature from 25 to 50 °C, is reported. With mechanistic modeling of water–polymer interactions, this unusual water sorption is attributed to the first-order phase transformation of PEG structures, and the key parameters for a more generalized strategy in materials development are identified. This work elucidates a new regime of water sorption with an unusual temperature dependence, enabling a promising engineering space for harnessing moisture and heat.

1. Introduction

Water vapor sorption from the atmosphere broadly impacts many fundamental processes in life science and physical systems.[1,2] On the one hand, the ability to capture moisture dictates the hydration state of tissues and plants in nature.[1] On the other hand, water sorption-based technologies that enable highly efficient capturing, production, and transport of water, have shown promising applications in dehumidification, energy storage, passive cooling, and freshwater production.[2–4] Understanding how to manipulate the behavior of sorbent materials is hence critical to enhance the potential of water sorption-based technologies.

Water sorption behavior typically can be quantified by the water uptake (w), which describes the mass of water vapor uptake per mass of dry sorbent materials at different relative humidities (RHs).[2] Temperature is one of the most significant factors for the water uptake of a specific sorbent material.[5] In general, water uptake decreases with the temperature rise due to the thermodynamic limit. At a higher temperature, there is an increased probability for adsorbed water molecules to escape because their kinetic energy due to thermal motion ($\sim k_B T$) increases (**Figure 1**a). Figure 1c shows the temperature sensitivity of water uptake for four representative sorbent materials including silica gels,[6,7] zeolites,[7] metal–organic frameworks (MOFs),[8] and hydrogels.[9,10] The temperature sensitivity, $\Delta w/\Delta T$, is defined as the ratio of the change of water uptake (Δw) to the corresponding temperature rise (ΔT). Most traditional sorbent materials show a negative $\Delta w/\Delta T$, indicating a decrease in water uptake due to increasing temperature (Figure 1c; Figure S1, Supporting Information). This behavior fundamentally limits the potential of water sorption for high-temperature applications.

Meanwhile, hydrogels have become an emerging material platform for water sorption.[11–13] In addition to their hydrophilicity, flexibility, and scalability, hydrogels hold significant promise because of their large tunability in water sorption properties.[14,15] By engineering the interaction between water and polymer at the molecular level, a range of water sorption capabilities and kinetics of hydrogels have been demonstrated and adapted for specific applications.[16–18] It is, therefore, highly desirable to further explore the engineering space of hydrogels, in particular to enhance water sorption with increasing temperature ($\Delta w/\Delta T > 0$).

In this work, we report an unusual temperature dependence of water sorption in semicrystalline hydrogels (Figure 1b), where water sorption is increased with elevated temperatures ($\Delta w/\Delta T > 0$, Figure 1c). Using a poly(ethylene glycol) (PEG) hydrogel as an example, we demonstrated that its water uptake at a high

X. Liu, L. Zhang, B. El Fil, C. D. Díaz-Marín, Y. Zhong, X. Li, E. N. Wang
Department of Mechanical Engineering
Massachusetts Institute of Technology
Cambridge, MA 02139, USA
E-mail: enwang@mit.edu
S. Lin
Department of Mechanical Engineering
Michigan State University
East Lansing, MI 48824, USA
E-mail: linshaot@msu.edu

The ORCID identification number(s) for the author(s) of this article can be found under https://doi.org/10.1002/adma.202211763

© 2023 The Authors. Advanced Materials published by Wiley-VCH GmbH. This is an open access article under the terms of the Creative Commons Attribution-NonCommercial-NoDerivs License, which permits use and distribution in any medium, provided the original work is properly cited, the use is non-commercial and no modifications or adaptations are made.

DOI: 10.1002/adma.202211763

15214095, 2023, 22, Downloaded from https://onlinelibrary.wiley.com/doi/10.1002/adma.202211763 by Michigan State University, Wiley Online Library on [28/09/2023]. See the Terms and Conditions (https://onlinelibrary.wiley.com/terms-and-conditions) on Wiley Online Library for rules of use; OA articles are governed by the applicable Creative Commons License

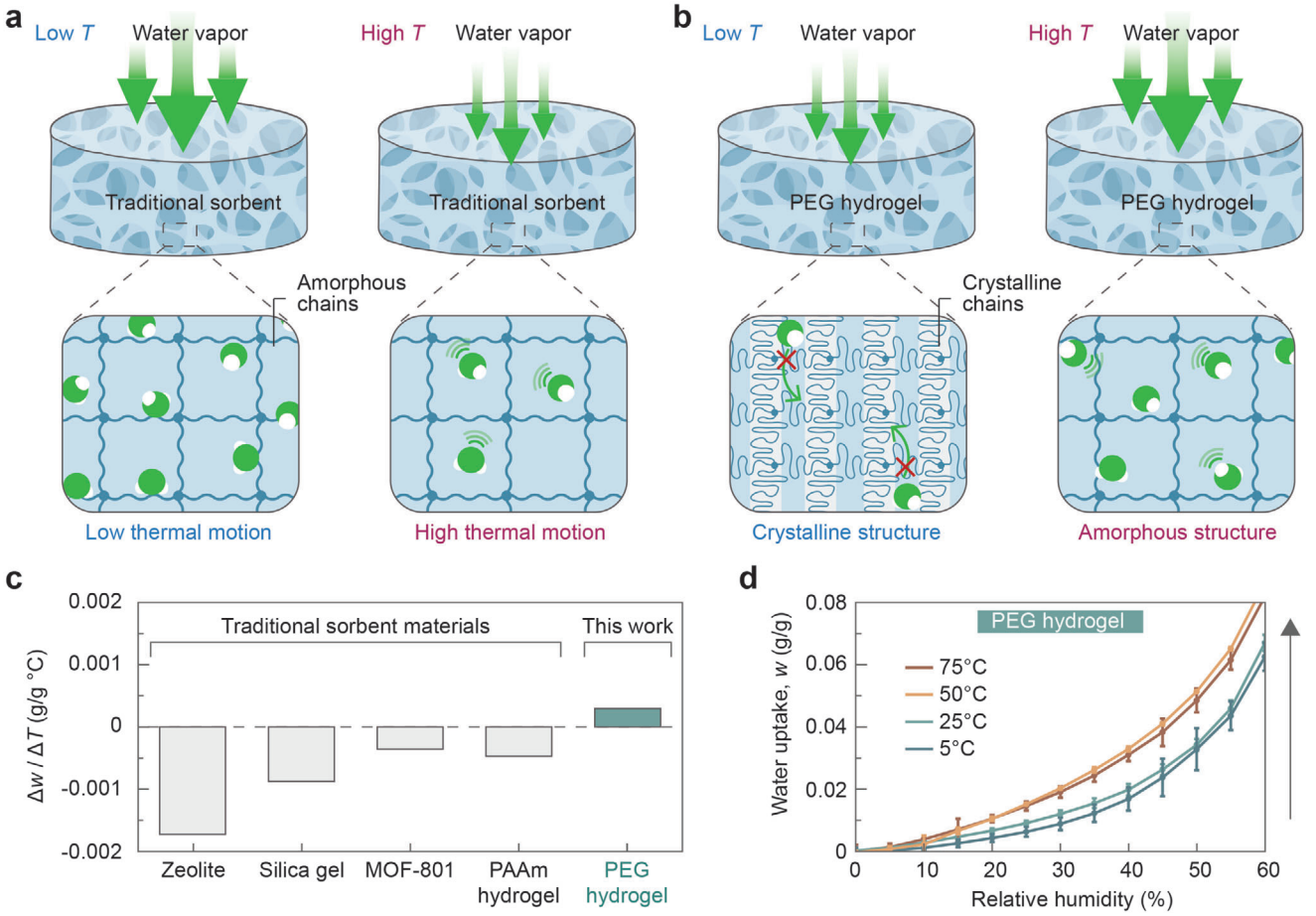


Figure 1. Dependence of water sorption on temperature. a) Schematic of traditional sorbents: sorption at a low temperature and desorption at a high temperature. b) Schematic of PEG hydrogels: desorption at a low temperature and sorption at a high temperature. The temperature-controlled phase transformation of nanocrystalline structures creates different interactions between the polymer and water molecules. When it is cooler than the melting point (T_m), the PEG chains are semicrystalline. When it is hotter than T_m, the PEG chains are amorphous. c) Comparison of the temperature sensitivity of water sorption of four representative traditional sorbent materials[3,6,7,9,19] and the PEG hydrogel. The water uptake change (Δw) is obtained at ≈40% RH and the temperature change (ΔT) is ≈ 50 °C. d) Water vapor uptake isotherms of the PEG hydrogel in g g^{-1} (g of water per g of the dried PEG hydrogel, w) as a function of RH at temperatures of 5, 25, 50, and 75 °C. Arrow: temperature increases. Error bars: standard deviations of three independent measurements.

temperature (50 °C) is much higher than that at room temperature (25 °C) (Figure 1d). With detailed characterizations of nanocrystalline structures in the polymer network, we observed that this unusual water sorption is associated with the first-order phase transformation of polymers from the semicrystalline state to the amorphous state (Figure 1b). Using mechanistic modeling, we showed how its thermodynamics is distinct from that of conventional water sorption. The melting of crystalline polymer chains induces additional changes in the partial molar free energy during the polymer mixing and deformation, leading to more water uptake at a higher temperature. Our measured water uptake at different RHs and temperatures shows good agreement with the thermodynamic analysis. With insights gained from the model, we identified three key parameters, i.e., adsorption enthalpy, polymer melting point, and crystallinity, that govern the temperature dependence of water sorption. This work presents a new material regime that shows an inverse temperature dependence of water sorption. Our results not only elucidate the underlying physics of water sorption in semicrystalline hydrogels but provide quantitative guidelines to further manipulate the temperature dependence of water sorption. These results pave the way toward various water sorption-based applications for a wide range of operating temperatures.

2. Results and Discussion

2.1. Structural Characterization of Crystalline-to-Amorphous Transition

Figure 2a shows a schematic of the crystalline polymer chains below the melting point and the amorphous polymer chains above the melting point. The transition between crystalline and amorphous polymer chains leads to distinct polymer–water interactions and potentially affects the water sorption. To understand the impact of crystalline-to-amorphous transition on the water uptake in hydrogels at higher temperatures (Figure 2a), we used

© 2023 The Authors. Advanced Materials published by Wiley-VCH GmbH

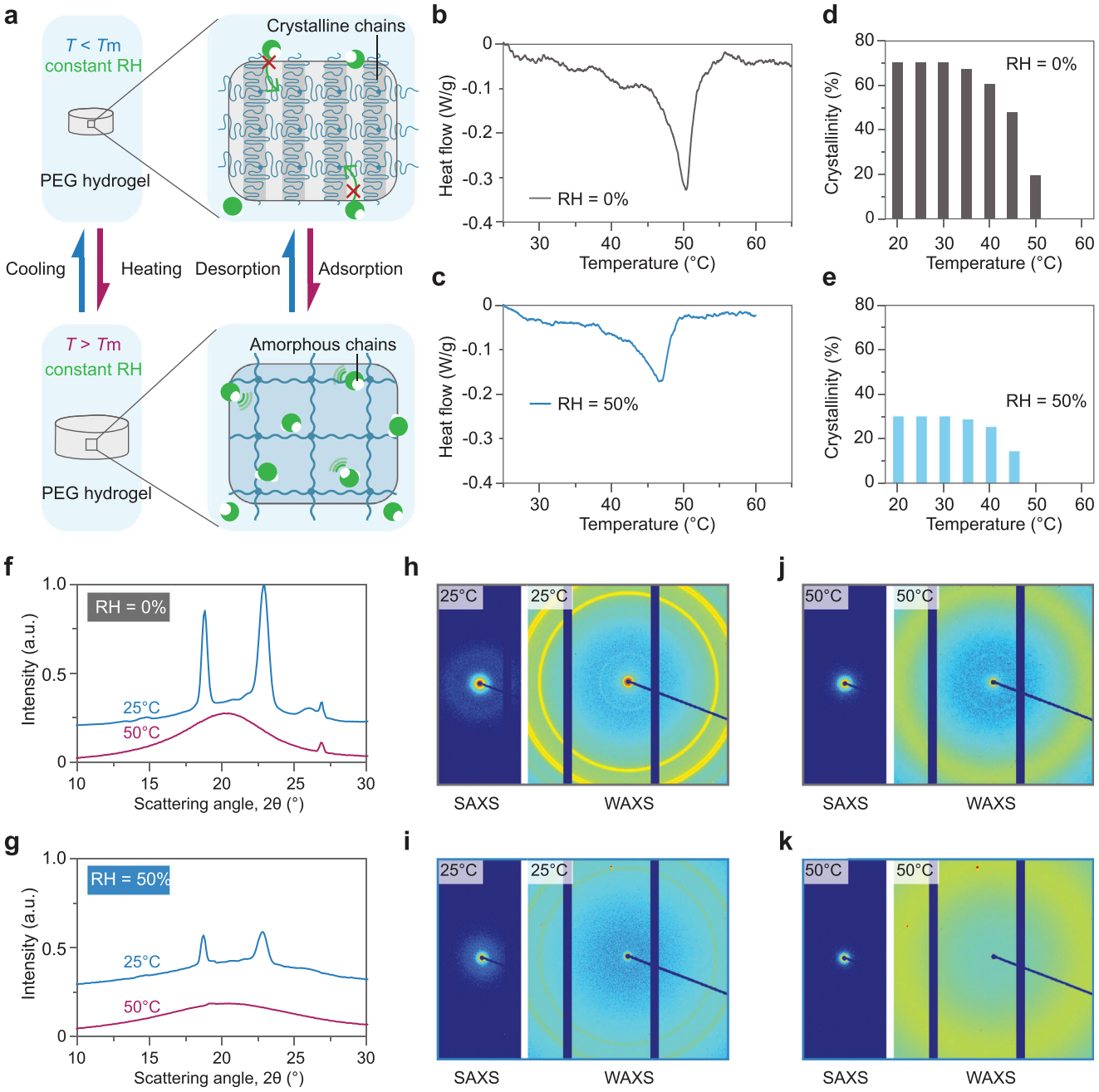


Figure 2. Evolution of polymer crystallinity in the semicrystalline hydrogel with temperature. a) Schematic of the PEG hydrogel desorbing at a low temperature ($T < T_m$) and adsorbing at a high temperature ($T > T_m$) under a constant RH. The polymer chains are semicrystalline when $T < T_m$, while the crystalline chains melt into amorphous chains when $T > T_m$. b) DSC thermograph of the PEG hydrogel when RH = 0%. c) DSC thermograph of the PEG hydrogel when RH = 50%. d) Crystallinity of the PEG hydrogel varying with different temperatures when RH = 0%. e) Crystallinity of the PEG hydrogel varying with different temperatures when RH = 50%. f) WAXS profiles of the PEG hydrogel at different temperatures when RH = 0%. g) WAXS profiles of the PEG hydrogel at different temperatures when RH = 50%. h) 2D SAXS and WAXS patterns of the PEG hydrogel at 25 °C ($T < T_m$) when RH = 0%. i) 2D SAXS and WAXS patterns of the PEG hydrogel at 25 °C ($T < T_m$) when RH = 50%. j) 2D SAXS and WAXS patterns of the PEG hydrogel at 50 °C ($T > T_m$) when RH = 0%. k) 2D SAXS and WAXS patterns of the PEG hydrogel at 50 °C ($T > T_m$) when RH = 50%.

a tetra-arm PEG hydrogel as the model material system (molecular weight: 10 kDa in each polymer chain between two chemical cross-linkers; see the Supporting Information for detailed synthesis).[20,21] Depending on the molecular weight, the melting point of PEG may vary from 1 to 66 °C,[22] falling in the temperature range where water exists in the liquid state at atmospheric pressure. In addition, the A-B type tetra-arm PEG hydrogel represents a homogeneous network structure of stereoregular polymer chains, ensuring the crystallization of polymer chains below the melting point.[20] At the nanoscale, the crystalline polymer chains

© 2023 The Authors. Advanced Materials published by Wiley-VCH GmbH

15214095, 2023, 22, Downloaded from https://onlinelibrary.wiley.com/doi/10.1002/adma.202211763 by Michigan State University, Wiley Online Library on [28/09/2023]. See the Terms and Conditions (https://onlinelibrary.wiley.com/terms-and-conditions) on Wiley Online Library for rules of use; OA articles are governed by the applicable Creative Commons License

are usually closely packed in parallel with one another, forming highly ordered regions called spherulites (Figure S2, Supporting Information), which are impermeable to water vapor. In contrast, amorphous polymer chains exhibit high mobility and high affinity with water.

We first quantified the crystallinity of PEG hydrogels at different RHs and temperatures using differential scanning calorimetry (DSC). We considered two representative RHs at 0% and 50%. When the RH was kept constant at 0% during the measurement, there was no water remaining in the material system. Increasing and maintaining the RH level inside the furnace at 50% led to significant water sorption in the hydrogel. The heat flow curves revealed the endothermic melting peaks (T_m) to be 51.2 °C at 0% RH and 46.5 °C at 50% RH (Figure 2b,c). The melting peaks decrease slightly when increasing the RH level inside the furnace, indicating that the moisture weakens PEG crystalline lamellae. The melting enthalpy of crystalline polymers $H_{melt}(RH,T)$ was determined by integrating the thermographic curve from 20 °C to T, and crystallinity can be calculated as $n_3\ (RH, T) = [H^{tot}_{melt}(RH) - H_{melt}(RH, T)]/H^0_{melt}$, where $H^{tot}_{melt}(RH)$ is the integration of the thermographic curve from 20 to 60 °C, and $H^0_{melt} = 165\ J\ g^{-1}$ is the enthalpy of fusion of 100% PEG crystal.[23] We obtained the crystallinity of the PEG hydrogel at specific conditions in Figure 2d,e. At both RHs (0% and 50%), the crystallinity showed a sharp transition only around the melting point; that is, when the temperature was far below T_m, it maintained a high crystallinity of 70% and 30%, respectively; when the temperature was far above T_m, all crystalline polymers disappeared due to the melting of crystalline lamellae (Figure 2d,e). When we did not control the RH to be constant in the testing furnace, a significant amount of water in hydrogels desorbed, leading to a broad peak around 120 °C in the calorimetry, which may interfere with the polymer melting peak (Figure S3, Supporting Information). In contrast to the polymer melting, the glass transition cannot change the polymer crystallinity, because it is a second-order phase transformation process. Instead, only the polymer chain stiffness varies across the glass transition temperature.[24]

To analyze the morphological evolution of crystalline polymers at different temperatures at the nanoscale, we performed X-ray scattering measurements on the PEG hydrogels at both 0% and 50% RHs. We first obtained 2D patterns of small-angle X-ray scattering (SAXS) and wide-angle X-ray scattering (WAXS), and then converted them to 1D profiles by conducting a circular average. In the 2D SAXS patterns (Figure 2h,i) and 1D SAXS profiles (Figure S4, Supporting Information) at 25 °C, the scattering peak (q^*) shifted from 0.48 to 0.24 nm^{-1}, when the RH increased from 0% to 50%. Based on Bragg's equation, we calculated the long period of the crystalline lamellae stacking to be $D = 2\pi/q^*$.[25] This indicated that the high RH led to a sparser distribution of PEG crystalline lamellae (D = 25.8 nm), compared to the one at a low RH (D = 13.1 nm). In contrast, no peaks were observed in the 2D SAXS patterns (Figure 2j,k) and 1D SAXS profiles (Figure S4, Supporting Information) at 50 °C for both RHs, since PEG crystalline lamellae were melted above T_m. In the 2D patterns of WAXS, two strong crystalline reflection rings were seen when the temperature was 25 °C (Figure 2h,i), and amorphous halos were presented when heated up to 50 °C (Figure 2j,k). For both RH levels at 25 °C, there were peaks located at 2θ = 18.8° and 22.9°, which represent the (120) and $(12\bar{4})/(\bar{1}24)$ planes of the crystalline lamellae, respectively (Figure 2f,g).[25] Furthermore, the increased RH led to a lower peak intensity, indicating a smaller size of crystalline lamellae. The size of the PEG crystalline lamellae L can be further estimated from the 1D WAXS profiles using the Scherrer equation $L = k\lambda/\beta\cos\theta$, where k is a dimensionless shape factor set as 0.9, λ is the wavelength of X-ray, β is the full width at half maximum of the peak in radians, and θ is the Braggs angle in radians.[26] When the RH increased from 0% to 50%, L measured at 2θ = 18.8° decreased from 17.6 to 10.9 nm (Figure 2f,g). The structural change of PEG hydrogels due to melting was also confirmed by polarized optical microscopy (POM), where we directly imaged the disappearance of spherulites at an elevated temperature and RH (Figure S2, Supporting Information). Observations obtained from the DSC, SAXS, WAXS, and POM consistently indicate that either a higher temperature or a higher RH results in lower crystallinity, lower density, and smaller size of the crystalline lamellae.

To further support the insights gained from the above microscopic characterizations, we performed mechanical and optical measurements of the crystalline-to-amorphous transition in PEG hydrogels at a macroscopic level. The stress–strain curves at various temperatures show the transition from a ductile to an elastomeric state due to the phase transformation of PEG hydrogels (Figure S5a, Supporting Information). When exposed to uniaxial tension at 25 °C and RH = 50%, PEG hydrogels first experienced elastic deformation with Young's modulus of 24 MPa, followed by plastic deformation when the strain was above the elastic limit (strain ϵ = 0.3). During the yielding process, some aligned fibrils emerged due to strain-induced crystallization (ϵ = 5, Figure S5b, Supporting Information). The mechanical responses above 50 °C were markedly different because of the melting of crystalline structures, exhibiting a much lower Young's modulus of 46 kPa. At elevated temperatures, hydrogels were highly deformable, while maintaining elasticity even when the uniaxial strain was above 10 (Figure S5c, Supporting Information). In addition, the UV–vis spectrophotometry provided the quantified light transmittance spectrum of a PEG hydrogel film at different temperatures (Figure S6, Supporting Information). In the visible light spectrum, the semicrystalline hydrogel at a low temperature (25 °C) showed low transmittance comparable to the amorphous hydrogel at higher temperatures (50 and 75 °C), due to the scattering centers formed by crystalline polymers at 25 °C.

2.2. Temperature-Dependent Water Sorption of Semicrystalline Hydrogels

To highlight the role of crystalline-to-amorphous transition and the resulting distinct temperature-dependent water sorption of PEG hydrogels, we synthesized a polyacrylamide (PAAm) hydrogel composed of a completely amorphous polymer network as a control sample for the PEG hydrogel. Owing to atactic polymer chains after crosslinking, the stereorandom polymers in the PAAm hydrogel cannot crystallize.[27] We characterized the water uptake and kinetics of both the PAAm and PEG hydrogels using a vapor sorption analyzer. Hydrogel samples were subjected to varying conditions of RH and temperature, and the resulting water uptake of hydrogels was measured gravimetrically. The kinetics of water sorption was quantified by a time constant, which

© 2023 The Authors. Advanced Materials published by Wiley-VCH GmbH

15214095, 2023, 22, Downloaded from https://onlinelibrary.wiley.com/doi/10.1002/adma.202211763 by Michigan State University, Wiley Online Library on [28/09/2023]. See the Terms and Conditions (https://onlinelibrary.wiley.com/terms-and-conditions) on Wiley Online Library for rules of use; OA articles are governed by the applicable Creative Commons License

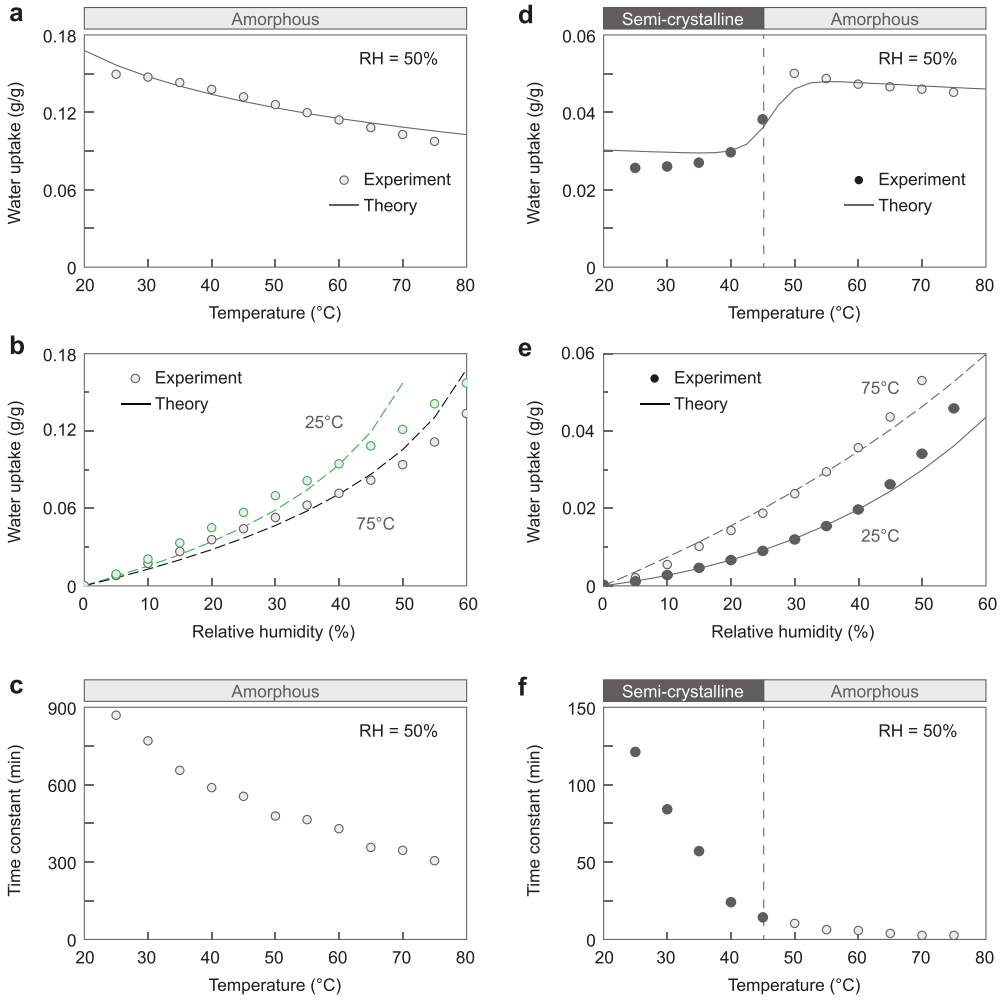


Figure 3. Comparison of the temperature-dependent water uptake between semicrystalline and fully amorphous hydrogels. a) Water uptake of the PAAm hydrogel (fully amorphous) as a function of temperature at RH = 50%. b) Water uptake of the PAAm hydrogel as a function of RH at $T = 25$ and 75 °C. c) Time constants of water uptake of the PAAm hydrogel as a function of temperature at RH = 50%. d) Water uptake of the PEG hydrogel (semicrystalline) as a function of temperature at RH = 50%. e) Water uptake of the PEG hydrogel as a function of RH at $T = 25$ and 75 °C. f) Time constants of water uptake of the PEG hydrogel as a function of temperature at RH of 50%.

is defined as the time duration when the water uptake increases from zero to a factor of (1-1/e) of its equilibrium mass gain, where e is Euler's number.

We first performed the vapor sorption analysis on the PAAm hydrogel. As expected, the PAAm hydrogel exhibited lower water uptake at higher temperatures (**Figure 3**a). For example, it adsorbed 0.15 g g^{-1} of water at 25 °C and 0.10 g g^{-1} at 75 °C, when the RH was 50% (Figure 3a,b). This conventional temperature dependence is attributed to the exothermic nature of water sorption.[28] Additionally, increased temperature enhances the vapor transport in the PAAm hydrogel.[16,17] Figure 3c shows that the time constant of water sorption by PAAm hydrogel gradually decreased from 14.5 to 5.0 h as the temperature increased from 25 to 75 °C.

We further performed vapor sorption analysis on the PEG hydrogels. With temperature-dependent crystalline-to-amorphous transformation, the water uptake of PEG hydrogels versus temperature exhibited an inverse trend ranging from 20 to 50 °C (Figure 3d,e). Specifically, when the RH was kept as 50%, the water uptake increased from 0.025 g g^{-1} at 25 °C to 0.050 g g^{-1} at 50 °C (Figure 3d). This result is because the crystalline polymers are densely stacked and inaccessible for water molecules at low temperatures. Within the temperature range of 20–50 °C, the higher temperature induced more amorphous polymers, which can imbibe more water. Note that the temperature for the transition in water sorption (Figure 3d) is in the same range as the crystalline-to-amorphous transition (e.g., 45 ± 5 °C at 50% RH, Figure 2e), indicating that the unusual water sorption behavior of PEG hydrogels is mainly governed by the phase transformation. When the temperature was above the melting point of PEG, the PEG hydrogel was completely amorphous (>50 °C). The exothermic sorption dominates the water uptake again, leading to the conventional temperature dependence similar to the PAAm hydrogel (Figure 3a,d). For the water uptake isotherms of PEG hydrogels in Figures 3e and 1d, the RH range is limited to 0–60%. Beyond 60% RH, the higher humidity leads to the melting of

© 2023 The Authors. Advanced Materials published by Wiley-VCH GmbH

15214095, 2023, 22, Downloaded from https://onlinelibrary.wiley.com/doi/10.1002/adma.202211763 by Michigan State University, Wiley Online Library on [28/09/2023]. See the Terms and Conditions (https://onlinelibrary.wiley.com/terms-and-conditions) on Wiley Online Library for rules of use; OA articles are governed by the applicable Creative Commons License

crystalline domains in the PEG hydrogels, and the temperature dependence returns to the conventional mode (Figure S7, Supporting Information).

On the other hand, distinct water uptake kinetics of the PEG hydrogel was also observed at different temperatures. The water sorption time constants decreased sharply from 124 to 11 min when the temperature increased from 25 to 50 °C (Figure 3f), which is due to the melting of crystalline polymers (Figure 2e,g). In addition, the sorption kinetics for PEG hydrogels (460 min at 50 °C) were generally much faster than that of PAAm hydrogels (11 min at 50 °C) even when they had the same dimensions (Figure 3c,f). The difference between the time constants of PAAm and PEG hydrogels can be attributed to the different chain mobility. Polymer chains in PAAm hydrogels remained in a glassy state (glass transition temperature, $T_g = 220$ °C) with very low mobility for water diffusion.[29] Even though the crystalline regions in PEG hydrogels were impermeable to water transport, polymer chains in the amorphous regions of PEG hydrogels were in a rubbery state ($T_g = -60$ °C) with high chain mobility for water diffusion in the amorphous regions.[30]

The comparison with amorphous PAAm hydrogels reflects the unusual behavior of PEG hydrogels in water sorption. Most polymer networks fail to show such inverse temperature dependence, because either they are hydrophobic polymers so that they cannot absorb water effectively or their melting temperatures are not between the freezing (0 °C at 1 atm) and boiling (100 °C at 1 atm) points of water to maintain absorbed water in the liquid state (Figure S8, Supporting Information). Referring to the material library, most common polymers such as PAAm, poly(vinyl alcohol), and poly(acrylic acid) present usual temperature-dependent water sorption (Figure S8, Supporting Information), while PEG (and its derivatives, Pluronic F127) is likely one of the few commercially available polymers showing the unique temperature dependence.[31,32] Although the amount of water vapor sorption for PEG hydrogels is relatively low (<0.1 g g^{-1}), hygroscopic salts and hydrophilic plasticizers can be potentially incorporated into the PEG hydrogel for regulating the interactions between the water vapor and PEG and further enhancing the water uptake.[11,33] Depending on the types and amounts of hygroscopic salts, the PEG–salt composites may exhibit different temperature-responsive water sorption behaviors.[11,33,34]

2.3. Theory for the Unusual Temperature Dependence of Water Sorption

We formulated a thermodynamic theory to elucidate the fundamentals of water uptake in semicrystalline hydrogels. In general, water vapor molecules in the humid air are first adsorbed and condense on the outmost surface of the dry polymers, and then the liquid water molecules on the surface start to mix with the amorphous polymer chains and further induce the volumetric expansion of the polymer network (Figure S9, Supporting Information).[17] Therefore, our theoretical framework accounts for the effects of vapor adsorption on the polymer surface, polymer–water mixing, polymer network deformation, and polymer melting. At equilibrium, the chemical potentials of water molecules in the gas phase $\mu_{1,\mathrm{gas}}$ and in the hydrogel $\mu_{1,\mathrm{hydrogel}}$ are balanced[15]

$$\mu_{1,\mathrm{gas}}(p,T) = \mu_{1,\mathrm{hydrogel}}(p,T) \tag{1}$$

where p is the vapor pressure. In the gas phase, the chemical potential of water molecules can be expressed as

$$\mu_{1,\mathrm{gas}}(p,T) = -\Delta H_{\mathrm{vap}}\left(1-\frac{T}{T_0}\right) + RT\ln(\mathrm{RH}) \tag{2}$$

where ΔH_{vap} is the enthalpy of vaporization of water at its boiling point T_0, and R is the gas constant. In the hydrogel sample, the chemical potential of water molecules is determined from the partial molar Gibbs free energy changes when water molecules transport from the gas phase to the hydrogel. Incorporating the multiple processes of water uptake, we can obtain

$$\mu_{1,\mathrm{hydrogel}}(p,T) = \left(\frac{\partial \Delta G_{\mathrm{ads}}}{\partial n_1}\right)_{\mathrm{p,T}} + \left(\frac{\partial \Delta G_{\mathrm{mix}}}{\partial n_1}\right)_{\mathrm{p,T}} + \left(\frac{\partial \Delta G_{\mathrm{def}}}{\partial n_1}\right)_{\mathrm{p,T}} + \left(\frac{\partial \Delta G_{\mathrm{melt}}}{\partial n_1}\right)_{\mathrm{p,T}} \tag{3}$$

where n_1 is the moles of water in the hydrogel, ΔG_{ads} is the Gibbs free energy change for adsorbing n_1 mol of water vapor on the surface of 1 mol of the dry hydrogel, ΔG_{mix} is the Gibbs free energy change for mixing n_1 mol of liquid water with 1 mol of the dry hydrogel, ΔG_{def} is the Gibbs free energy change for deforming the polymer chains in 1 mol of the dry hydrogel due to water uptake, and ΔG_{melt} is the Gibbs free energy change for melting the crystalline polymer in 1 mol of the dry hydrogel.

Specifically, the partial molar Gibbs free energy change due to the sorption is associated with the monolayer adsorption and multilayer liquefaction on the polymer surface, which can be described by

$$\left(\frac{\partial \Delta G_{\mathrm{ads}}}{\partial n_1}\right)_{\mathrm{p,T}} = -\Delta H_{\mathrm{vap}}\left(1-\frac{T}{T_0}\right) - RT\ln c \tag{4}$$

where c is the Brunauer–Emmett–Teller (BET) constant describing the energy difference between monolayer adsorption and multilayer liquefaction, and $c = \exp((\Delta H_{\mathrm{liq}} - \Delta H_{\mathrm{ads}})/RT)$,[35] where ΔH_{ads} is the molar enthalpy of water adsorption on the hydrogel surface, and ΔH_{liq} is the molar enthalpy of water condensation (i.e., $\Delta H_{\mathrm{liq}} = -\Delta H_{\mathrm{vap}}$). Note that the above adsorption mechanism described by Equation (4) is a unique process associated with vapor molecule–polymer surface interaction, which is not involved in the conventional interactions between liquid molecule and bulk polymer, such as swelling and dissolution. Derived from the Flory–Huggins theory,[36,37] the partial molar Gibbs free energy change due to the mixing between amorphous polymers and water is

$$\left(\frac{\partial \Delta G_{\mathrm{mix}}}{\partial n_1}\right)_{\mathrm{p,T}} = RT\left[ln\frac{1}{1+\frac{(1-n_3)}{w}} + \left(1-\frac{1}{1+\frac{(1-n_3)}{w}}\right) + \chi\left(1-\frac{1}{1+\frac{(1-n_3)}{w}}\right)^2\right] \tag{5}$$

© 2023 The Authors. Advanced Materials published by Wiley-VCH GmbH

15214095, 2023, 22, Downloaded from https://onlinelibrary.wiley.com/doi/10.1002/adma.202211763 by Michigan State University, Wiley Online Library on [28/09/2023]. See the Terms and Conditions (https://onlinelibrary.wiley.com/terms-and-conditions) on Wiley Online Library for rules of use; OA articles are governed by the applicable Creative Commons License

where n_3 is the crystallinity of polymer chains in the hydrogel, w is the water uptake of the dry hydrogel, and χ is the interaction parameter between amorphous polymers and water. Based on the rubber elasticity,[38] the partial molar Gibbs free energy change due to polymer deformation can be expressed as

$$\left(\frac{\partial \Delta G_{\text{def}}}{\partial n_1}\right)_{\text{p,T}} = \frac{EV_1}{3}\left(1 - \frac{1}{2(1+w)^{2/3}}\right) \tag{6}$$

where E is the Young's modulus of the hydrogel and V_1 is the molar volume of water. Note that in the PEG hydrogel, both chemical crosslinking and physical crosslinking (i.e., crystalline lamellae) contribute to the hydrogel elasticity. Assuming that the melting of crystalline polymers per mol of the dry hydrogel is independent of the water content, the partial molar Gibbs free energy change due to polymer melting is 0

$$\left(\frac{\partial \Delta G_{\text{melt}}}{\partial n_1}\right)_{\text{p,T}} = 0 \tag{7}$$

Substituting Equations (2–7) into Equation (1), we arrived at an equation describing the water uptake of hydrogels as a function of RH and T.

$$\ln(\text{RH}) = -\left(\frac{\Delta H_{\text{liq}} - \Delta H_{\text{ads}}}{RT}\right) + \ln\left(\frac{1}{1+\frac{(1-n_3)}{w}}\right) + \left(\frac{\frac{(1-n_3)}{w}}{1+\frac{(1-n_3)}{w}}\right) + \chi\left(\frac{\frac{(1-n_3)}{w}}{1+\frac{(1-n_3)}{w}}\right)^2 + \frac{E\widehat{V}_1}{3RT}\left(1 - \frac{1}{2(1+w)^{2/3}}\right) \tag{8}$$

With known numerical quantities of n_3, E, ΔH_{ads}, and χ (Table S1 and Figures S10 and S11, Supporting Information), Equation (8) was solved numerically. Note that Equation (8) is valid for both semicrystalline hydrogels and amorphous hydrogels. For the water sorption of amorphous hydrogels, n_3 is zero for all RH and T. We plotted the theoretically calculated water uptake versus temperature and RH for the PAAm hydrogel (Figure 3a,b) and PEG hydrogel (Figure 3d,e). The water uptake of both hydrogels showed good agreement with experimental data. For the PEG hydrogel, the thermodynamic theory also predicts the increased water uptake with the temperature rise at 30–45 °C due to crystalline-to-amorphous structural change (Figure 3d,e). Inserting the calculated water uptake back to Equation (3), we quantified how the thermodynamics of semicrystalline hydrogels is fundamentally different from that of fully amorphous hydrogels. In particular, the existence and evolution of crystalline polymer chains induce additional changes in chemical potentials during the polymer mixing $\partial \Delta G_{\text{mix}}/\partial n_1$ and deformation $\partial \Delta G_{\text{def}}/\partial n_1$ (Figure S12, Supporting Information), which is the physical origin of this unusual temperature-dependent water sorption behavior. As a result, these changes lead to more water uptake at a higher temperature, compared to that at room temperature.

2.4. Engineering Space for Water Sorption of Semicrystalline Hydrogels

With our thermodynamic model, we demonstrate the tunability of the unusual temperature-dependent water sorption by evaluating the effects of various parameters on the final water uptake at different temperatures. First, we studied the role of water–polymer interaction in water sorption of semicrystalline hydrogels. Specifically, $(\Delta H_{\text{ads}} - \Delta H_{\text{liq}})$ represents the enthalpy difference between the first-layer of water adsorption and multilayer water condensation. The smaller quantity of $(\Delta H_{\text{ads}} - \Delta H_{\text{liq}})$ indicates a more negative value of adsorption enthalpy and a stronger affinity between the water vapor and hydrogel surface. As predicted by our theory, the decrease of $(\Delta H_{\text{ads}} - \Delta H_{\text{liq}})$ from −0.4 to −2.4 kJ mol^{-1} not only enhances the water uptake in the full range of operating temperature, but also enlarges the difference of water uptakes between the semicrystalline and amorphous states (**Figure 4**a; Figure S13a, Supporting Information). χ, another quantity that describes the interaction between liquid water and polymers during mixing, follows the similar trend as $(\Delta H_{\text{ads}} - \Delta H_{\text{liq}})$; that is, a lower value of χ leads to higher uptake among all temperatures (Figure S13b, Supporting Information). For melted hydrogels above T_{m}, the slope in the plot of normalized water uptake versus temperature increases with the decrease of $(\Delta H_{\text{ads}} - \Delta H_{\text{liq}})$ (Figure S13c, Supporting Information), while remaining independent of χ (Figure S13d, Supporting Information).

Besides the parameters describing the interaction between water and polymer (e.g., $\Delta H_{\text{ads}} - \Delta H_{\text{liq}}$ and χ), we also investigated the effect of material parameters, in particular, the melting point (T_{m}) and maximum crystallinity ($n_{3,\text{max}}$) of crystalline polymers. The increase of T_{m} right shifted the transition point in water uptake versus temperature (Figure 4b) due to the change of the temperature-dependent crystallinity and Young's modulus (Figure S14a,b, Supporting Information). For the temperature range of 20–70 °C, the hydrogel will exhibit a uniformly high water uptake if $T_{\text{m}} = 10$ °C, and a uniformly low water uptake if $T_{\text{m}} = 70$ °C. If we keep a constant melting point but vary the maximum level of crystallinity from 0% to 70%, the transition of water uptake between the semicrystalline and amorphous state will become more significant (Figure 4c; Figure S14c,d, Supporting Information). Practically, we found that the polymer melting point (T_{m}) and maximum crystallinity ($n_{3,\text{max}}$) can be well-controlled by engineering the chain length of polymer networks. We tested the crystalline-to-amorphous transition and the resulting water sorption behaviors of PEG hydrogels with different polymer chain lengths (Table S2, Supporting Information). When the polymer chain length between two chemical cross-linkers increased from 5 to 40 kDa, T_{m} and $n_{3,\text{max}}$ increased from 25.6 °C and 0.44 to 53.6 °C and 0.78, respectively (Table S2, Supporting Information). The rise of melting point led to a right shift of the water sorption curve (Figure S15a–c, Supporting Information), as well captured by the model predictions in Figure 4b. On the other hand, we showed that the larger maximum crystallinity resulted in the sharper change in water sorption around melting temperature (Figure S15a–c, Supporting Information), which is consistent with the modeling results in Figure 4c. This proof-of-concept experiment further demonstrates the large engineering space for the water sorption behavior of semicrystalline hydrogels and

© 2023 The Authors. Advanced Materials published by Wiley-VCH GmbH

15214095, 2023, 22, Downloaded from https://onlinelibrary.wiley.com/doi/10.1002/adma.202211763 by Michigan State University, Wiley Online Library on [28/09/2023]. See the Terms and Conditions (https://onlinelibrary.wiley.com/terms-and-conditions) on Wiley Online Library for rules of use; OA articles are governed by the applicable Creative Commons License

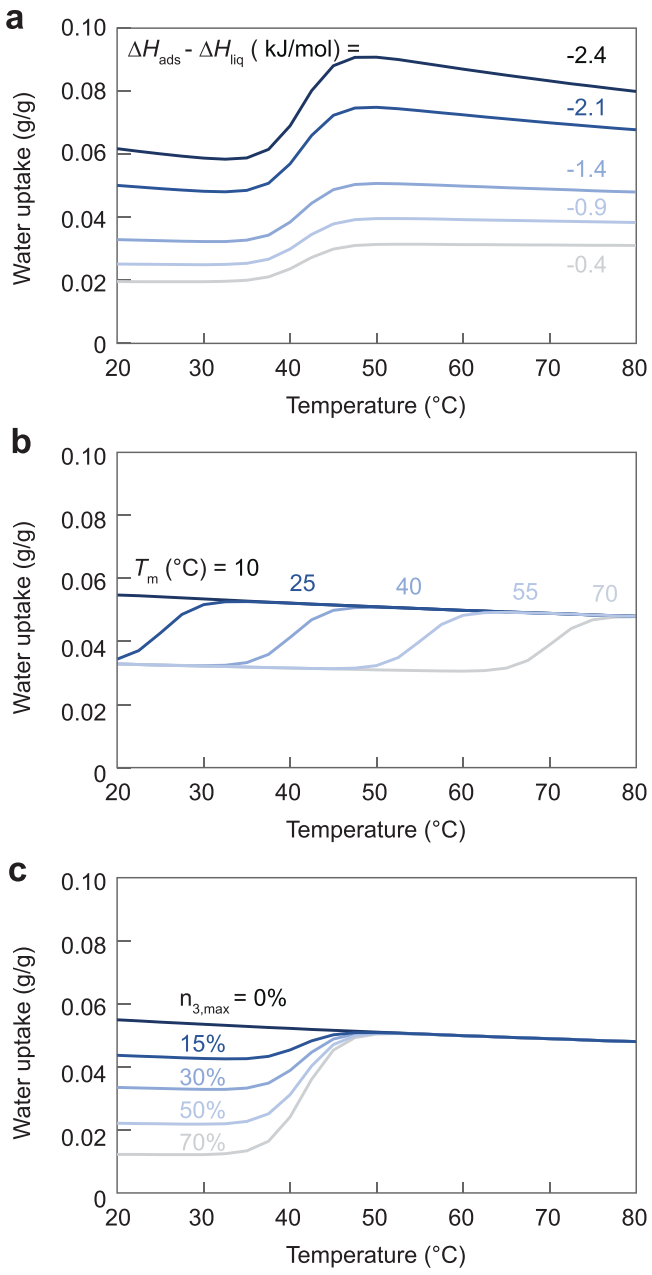


Figure 4. Theoretical water uptake of the semicrystalline hydrogel as a function of temperature in response to the changing design parameters. a–c) Parametric analysis of the enthalpy difference between adsorption and condensation ($\Delta H_{ads} - \Delta H_{liq}$) (a), the melting point of the polymers (T_m) (b), and the maximum polymer crystallinity ($n_{3,max}$) (c).

confirms the validity of using the developed thermodynamic model to guide the practical design, where we can rationally achieve the targeted water uptake behavior through the inverse design of adsorption enthalpy, polymer–water interaction parameter, melting point, and crystallinity. In contrast to $\Delta H_{ads} - \Delta H_{liq}$, χ, T_m, and $n_{3,max}$, we showed that the polymer mass ratio during sample preparation had negligible effects on water sorption (Table S3 and Figure S15d–f, Supporting Information) because the hydrogel was fully dried before the water sorption tests regardless of the initial amount of water. In addition to temperature, other physical variables (e.g., the mechanical stress, co-solvent, light, and electric field) that can trigger the structural transformation in semicrystalline hydrogels are highly desirable to modulate the water sorption behavior.[39]

3. Conclusion

We have reported an unusual sorption behavior in semicrystalline hydrogels, where water sorption increases with temperature. Using a semicrystalline PEG hydrogel as a typical material system, we showed that its water uptake at an elevated temperature (50 °C, 50% RH) is twice as high as that at room temperature (25 °C, 50% RH). Through systematic characterization on thermal, structural, mechanical, and optical performances of the nanocrystalline structures in PEG hydrogels at different temperatures and RHs, we showed that the increased water uptake at a higher temperature is due to the crystalline-to-amorphous transition of polymers. To further elucidate the underlying physics, we developed a mechanistic model that couples the melting, mixing, and deformation of semicrystalline polymers with the water sorption process. Our model showed that the temperature dependence of water sorption of semicrystalline hydrogels is fundamentally determined by both properties of crystalline polymers (e.g., melting point and crystallinity) and interactions between amorphous polymers and water molecules (e.g., adsorption enthalpy and polymer–water interaction parameter). Specifically, the melting of crystalline polymer chains induces additional changes in the partial molar free energy during the polymer mixing and deformation, leading to more water uptake at a higher temperature.

Our findings provide generalized molecular design principles to realize an inverse temperature dependence of water sorption, indicating a large engineering space to further manipulate the water sorption of hydrogels. While this work focused on a specific material system of PEG hydrogels controlled by temperature, our analysis can be extended to understanding and engineering the water sorption of hydrogels that experience different thermoresponsive physical transitions, such as glass transition and coil-to-globule transition, or hydrogels that are responsive to various external stimuli, such as mechanical stress and electrical field. In addition, we believe the unusual temperature-dependent sorption behavior will enable a new degree of freedom to harness moisture and heat, promising the development of various water sorption-based technologies in humidity regulation, energy storage, thermal management, and water harvesting, among others.

4. Experimental Section

Synthesis of PEG Hydrogels: The PEG hydrogel was synthesized from tetra-amine-terminated PEG macromers (4-arm-PEG-amine, 20 000 g mol^{-1}, Laysan Bio) and tetra-NHS-terminated PEG macromers (4-arm-PEG-NHS, 20 000 g mol^{-1}, Laysan Bio), following the reported protocol. First, 100 mg of PEG-amine was dissolved in 1 mL phosphate buffer solution with a pH of 7.4 and ionic strength of 100 mM. Then, 100 mg of PEG-NHS was dissolved in 1 mL of phosphate-citric acid buffer solution with a pH of 5.8 and ionic strength of 100 mM. Thereafter, both the solutions of PEG-amine and PEG-NHS were vigorously mixed and poured into a rectangular mold with the thickness of 1.5 mm. The

© 2023 The Authors. Advanced Materials published by Wiley-VCH GmbH

15214095, 2023, 22, Downloaded from https://onlinelibrary.wiley.com/doi/10.1002/adma.202211763 by Michigan State University, Wiley Online Library on [28/09/2023]. See the Terms and Conditions (https://onlinelibrary.wiley.com/terms-and-conditions) on Wiley Online Library for rules of use; OA articles are governed by the applicable Creative Commons License

final concentration of PEG-based macromers was 100 g L^{-1}, nearly at the overlap concentration of PEG macromers. After incubation at room temperature for 2 h, the A-B type tetra-arm PEG hydrogel was generated with the molecular weight of each effective strand as 10 000 g mol^{-1}. The PEG hydrogel was dried in an environmental chamber (RH = 0%) overnight to get a dry PEG hydrogel. The thickness after drying was ≈ 0.7 mm, measured by a caliper.

To prepare PEG hydrogels with different polymer chain lengths, different tetra-amine-terminated PEG macromers (4-arm-PEG-amine, 5000, 10 000, or 40 000 g mol^{-1}, JenKem Technology USA) and different tetra-NHS-terminated PEG macromers (4-arm-PEG-NHS, 5000, 10 000, or 40 000 g mol^{-1}, JenKem Technology USA) were used, and the synthesis followed the abovementioned procedure. Note that all of the PEG macromers obtained from Laysan Bio or JenKem Technology USA had a polydispersity of less than 1.07. To prepare PEG hydrogels with different PEG mass ratios, the same tetra-amine-terminated PEG macromers (4-arm-PEG-amine, 20 000 g mol^{-1}, Laysan Bio) and tetra-NHS-terminated PEG macromers (4-arm-PEG-NHS, 20 000 g mol^{-1}, Laysan Bio) were used. Then, different amounts of PEG-amine (50 mg or 150 mg) were dissolved in 1 mL phosphate buffer solution, and different amounts of PEG-NHS (50 mg or 150 mg) in 1 mL of phosphate–citric acid buffer solution, and the synthesis followed the abovementioned procedure.

Synthesis of PAAm Hydrogels: The PAAm hydrogel was synthesized from radical polymerization of acrylamide (AAm, Sigma-Aldrich) and *N*,*N*'-methylenebisacrylamide (MBAA, Sigma-Aldrich). First, 1 g of AAm, 10 mg of MBAA, and 22.8 mg of ammonium persulfate (APS, Sigma-Aldrich) were dissolved in 10 mL of water. Oxygen was removed from the solution through nitrogen purging for 10 min. Then, 10 µL of *N*,*N*,*N*′,*N*′-tetramethylethylenediamine (TEMED, Sigma-Aldrich) was vigorously mixed in the solution and poured into a rectangular mold with a thickness of 1.5 mm. After incubation at 50 °C for 2 h, the PAAm hydrogel was generated with the molecular weight of each effective strand as 10 000 g mol^{-1}. The PAAm hydrogel was dried in an environmental chamber (RH = 0%) overnight to get a dry PAAm hydrogel. The thickness after drying was ≈0.7 mm.

Vapor Sorption Analysis: The water sorption capability and kinetics of hydrogels were characterized via a vapor sorption analyzer (Q5000SA, TA Instruments). The plots of water uptake versus temperature were measured at a fixed level of relative humidity (RH) and varied temperatures ranging from 25 to 75 °C. The plots of water uptake versus RH were measured at a fixed temperature and varied RHs ranging from 0% to 90%. The capability of water uptake was calculated by the equilibrium mass gain per gram of dry hydrogel. The time constant τ of water uptake was calculated by fitting the mass gain curve to the following equation:

$$\frac{m(t) - m(0)}{m(\infty) - m(0)} = 1 - e^{-t/\tau} \tag{9}$$

where $m(t)$ is the mass at time t after water vapor sorption, $m(0)$ is the initial mass before water vapor sorption, and $m(\infty)$ is the equilibrium mass after water vapor sorption. The value of $m(\infty)$ is determined by the mass when $\frac{dm(t)}{dt} \leq 0.005\% \times m(0)$.

X-ray Scattering Measurement: To perform the X-ray scattering measurement under specific conditions, the hydrogel film was pre-incubated at a certain temperature (25 or 50 °C) and RH (0% or 50%) for 12 h, and then transferred to a sealed sample cell holder with mica windows on a temperature-controlled stage. The SAXS and WAXS measurement was performed using Ni-filtered CuKa1 radiation with an X-ray wavelength of 0.154 nm and a Pilatus3R 300K detector (Dectris) in a SAXSLAB instrument. A small-angle 2 mm beamstop with a sample-detector distance of 1059.1 mm was used for SAXS, and a wide-angle 2 mm beamstop with a sample-detector distance of 109.1 mm was used for WAXS. The exposure time was set as 300 s. Raw SAXS and WAXS patterns were processed with corrections by the MATLAB-based GIXSGUI toolbox. The 2D-SAXS and 2D-WAXS patterns were further converted to 1D profiles by conducting a circular average.

Polarized Optical Microscopy: A polarized optical microscope (Zeiss Axioscope, POL mode) was used to characterize the organization of polymer crystalline lamellae at different temperatures (25, 50, or 75 °C) and RH (50%). The images were taken by the ZEN software with a constant exposure time of 100 ms.

Differential Scanning Calorimetry: To measure the crystallinity under varied conditions, a TGA/DSC (Mettler Toledo) coupled to the MHG32 humidity generator (ProUmid) was used to study the heat flow at a constant RH (0%, 25%, or 50%). Around 7 mg of the PEG hydrogel was placed into an open Alox crucible for the TGA/DSC measurement. The sample in the TGA/DSC underwent heating–cooling–heating cycles between 25 and 85 °C (or between 25 and 60 °C, depending on the RH) at 1 °C min^{-1}. The atmosphere was humid nitrogen with a flow rate of 8 mL min^{-1}. In addition, DSC (Discovery) alone was used to expose hydrogels to pure nitrogen and study the heat flow due to both polymer and water. The hydrogels were pre-incubated at a certain temperature (25 °C) and RH (0% or 50%) for 12 h. Around 5 mg of the PEG hydrogel was placed in a Tzero Pan for the DSC measurement. The sample in the DSC underwent heating–cooling–heating cycles between 0 and 150 °C at 5 °C min^{-1}. The atmosphere was pure nitrogen with a flow rate of 30 mL min^{-1}.

Tensile Test: The mechanical properties of PEG hydrogels were characterized by a pure-shear test.[20] The hydrogel samples were first pre-incubated at a certain temperature (25, 50, or 75 °C) and RH (50%) for 12 h, and stretched in an oil bath at the same temperatures (25, 50, or 75 °C) using a uniaxial benchtop mechanical tester (UStretch, CellScale). The samples had the dimensions of 4.48 mm in width, 2.74 mm in gauge length, and 0.7 mm in thickness, which were measured using a caliper.

UV–Vis Transmittance: The transmission spectra (200–1000 nm) of the hydrogel membranes were measured by a UV–vis spectrophotometer (Evolution 60S, Thermo Fisher Scientific). The hydrogel samples (≈ 0.7 mm in thickness) were first pre-incubated at a certain temperature (25, 50, or 75 °C) and RH (50%) for 12 h, and then transferred to the silicone oil for measurement. The UV–vis spectrum of silicone oil was used as the background spectrum.

Supporting Information

Supporting Information is available from the Wiley Online Library or from the author.

Acknowledgements

X.L. and L.Z. contributed equally to this work. This material is based upon work supported by the U.S. Department of Energy's Office of Energy Efficiency and Renewable Energy (EERE), under the grant no. DE-EE0009679 with Sven Mumme as the program manager. The authors also gratefully acknowledge technical discussions with Prof. Xuanhe Zhao, Prof. Gang Chen, Chase Hartquist, James Zhang, Dr. Yaodong Tu at MIT, and Dr. Caleb B. McDonald at Mettler-Toledo.

Conflict of Interest

The authors declare no conflict of interest.

Data Availability Statement

The data that support the findings of this study are available from the corresponding author upon reasonable request.

Keywords

hydrogels, phase transformation, temperature dependence, vapor sorption, water harvesting

Received: December 15, 2022
Revised: February 13, 2023
Published online: April 18, 2023

© 2023 The Authors. Advanced Materials published by Wiley-VCH GmbH

15214095, 2023, 22, Downloaded from https://onlinelibrary.wiley.com/doi/10.1002/adma.202211763 by Michigan State University, Wiley Online Library on [28/09/2023]. See the Terms and Conditions (https://onlinelibrary.wiley.com/terms-and-conditions) on Wiley Online Library for rules of use; OA articles are governed by the applicable Creative Commons License

[1] a) M. Sawka, W. Latzka, R. Matott, S. Montain, *Int. J. Sports Med.* **1998**, *19*, S108; b) N. A. Aviara, in *Sorption in 2020s*, IntechOpen, London, UK **2020**, p. 145.
[2] A. LaPotin, H. Kim, S. R. Rao, E. N. Wang, *Acc. Chem. Res.* **2019**, *52*, 1588.
[3] H. Kim, S. R. Rao, E. A. Kapustin, L. Zhao, S. Yang, O. M. Yaghi, E. N. Wang, *Nat. Commun.* **2018**, *9*, 1191.
[4] a) S. Cui, C. Ahn, M. C. Wingert, D. Leung, S. Cai, R. Chen, *Appl. Energy* **2016**, *168*, 332; b) Y. Zheng, H. Bai, Z. Huang, X. Tian, F.-Q. Nie, Y. Zhao, J. Zhai, L. Jiang, *Nature* **2010**, *463*, 640.
[5] S. Shimizu, N. Matubayasi, *Langmuir* **2021**, *37*, 11008.
[6] S. Dini, Ph.D. Thesis, Illinois Institute of Technology, Chicago, IL, USA **1981**.
[7] Y. Wang, M. D. LeVan, *J. Chem. Eng. Data* **2009**, *54*, 2839.
[8] H. Kim, S. Yang, S. R. Rao, S. Narayanan, E. A. Kapustin, H. Furukawa, A. S. Umans, O. M. Yaghi, E. N. Wang, *Science* **2017**, *356*, 430.
[9] P. A. Kallenberger, M. Fröba, *Commun. Chem.* **2018**, *1*, 28.
[10] a) H. Lu, W. Shi, J. H. Zhang, A. C. Chen, W. Guan, C. Lei, J. R. Greer, S. V. Boriskina, G. Yu, *Adv. Mater.* **2022**, *34*, 2205344; b) H. Lu, W. Shi, Y. Guo, W. Guan, C. Lei, G. Yu, *Adv. Mater.* **2022**, *34*, 2110079; c) W. Shi, W. Guan, C. Lei, G. Yu, *Angew. Chem., Int. Ed.* **2022**, e202211267.
[11] Y. Guo, W. Guan, C. Lei, H. Lu, W. Shi, G. Yu, *Nat. Commun.* **2022**, *13*, 2761.
[12] a) X. Xu, S. Ozden, N. Bizmark, C. B. Arnold, S. S. Datta, R. D. Priestley, *Adv. Mater.* **2021**, *33*, 2007833; b) D. K. Nandakumar, Y. Zhang, S. K. Ravi, N. Guo, C. Zhang, S. C. Tan, *Adv. Mater.* **2019**, *31*, 1806730.
[13] I. Haechler, H. Park, G. Schnoering, T. Gulich, M. Rohner, A. Tripathy, A. Milionis, T. M. Schutzius, D. Poulikakos, *Sci. Adv.* **2021**, *7*, abf3978.
[14] X. Liu, J. Liu, S. Lin, X. Zhao, *Mater. Today* **2020**, *36*, 102.
[15] G. Chen, *Phys. Chem. Chem. Phys.* **2022**, *24*, 12329.
[16] C. D. Díaz-Marín, L. Zhang, B. El Fil, Z. Lu, M. Alshrah, J. C. Grossman, E. N. Wang, *Int. J. Heat Mass Transfer* **2022**, *195*, 123103.
[17] C. D. Díaz-Marín, L. Zhang, Z. Lu, M. Alshrah, J. C. Grossman, E. N. Wang, *Nano Lett.* **2022**, *22*, 1100.
[18] Y. Guo, J. Bae, Z. Fang, P. Li, F. Zhao, G. Yu, *Chem. Rev.* **2020**, *120*, 7642.
[19] H. Mittal, A. Al Alili, S. M. Alhassan, *Microporous Mesoporous Materials* **2020**, *299*, 110106.
[20] S. Lin, J. Ni, D. Zheng, X. Zhao, *Extreme Mech. Lett.* **2021**, *48*, 101399.
[21] N. A. Peppas, K. B. Keys, M. Torres-Lugo, A. M. Lowman, *J. Controlled Release* **1999**, *62*, 81.
[22] A. A. D'souza, R. Shegokar, *Expert Opin. Drug Delivery* **2016**, *13*, 1257.
[23] K. Pielichowski, K. Flejtuch, *Polym. Adv. Technol.* **2002**, *13*, 690.
[24] J. Gibbs, E. DiMarzio, *J. Polym. Sci., Part B: Polym. Phys.* **1987**, *25*, 1949.
[25] A. Banpean, H. Takagi, N. Shimizu, N. Igarashi, S. Sakurai, *Polymer* **2021**, *229*, 123971.
[26] S. Lin, X. Liu, J. Liu, H. Yuk, H.-C. Loh, G. A. Parada, C. Settens, J. Song, A. Masic, G. H. McKinley, *Sci. Adv.* **2019**, *5*, eaau8528.
[27] C. B. Crawford, B. Quinn, in *Microplastic Pollutants* (Eds: C. B. Crawford, B. Quinn), Elsevier, New York **2017**, p. 57.
[28] V. J. Inglezakis, S. G. Poulopoulos, in *Adsorption, Ion Exchange and Catalysis*, (Eds: V. J. Inglezakis, S. G. Poulopoulos), Elsevier, Amsterdam, The Netherlands **2006**, p. 243.
[29] I. Neamtu, A. Chiriac, L. Nita, *Adv. Mater.* **2006**, *8*, 1939.
[30] P. Törmälä, *Eur. Polym. J.* **1974**, *10*, 519.
[31] P. C. Hiemenz, T. P. Lodge, in *Polymer Chemistry*, CRC Press, Boca Raton, FL, USA **2007**.
[32] C. M. Hassan, N. A. Peppas, in *Biopolymers: PVA Hydrogels, Anionic Polymerisation Nanocomposites*, Springer, Berlin/Heidelberg, Germany **2000**, p. 37.
[33] F. Ni, N. Qiu, P. Xiao, C. Zhang, Y. Jian, Y. Liang, W. Xie, L. Yan, T. Chen, *Angew. Chem., Int. Ed.* **2020**, *59*, 19237.
[34] R. Magin, B. Mangum, J. Statler, D. Thornton, *J. Res. Natl. Bur. Stand.* **1981**, *86*, 181.
[35] S. Brunauer, P. H. Emmett, E. Teller, *J. Am. Chem. Soc.* **1938**, *60*, 309.
[36] a) P. J. Flory, *J. Chem. Phys.* **1942**, *10*, 51; b) M. L. Huggins, *J. Chem. Phys.* **1941**, *9*, 440.
[37] W. Hong, X. Zhao, J. Zhou, Z. Suo, *J. Mech. Phys. Solids* **2008**, *56*, 1779.
[38] P. J. Flory, J. Rehner Jr, *J. Chem. Phys.* **1943**, *11*, 512.
[39] a) I. Rao, K. Rajagopal, *Int. J. Solids Struct.* **2001**, *38*, 1149; b) A. Gupper, K. A. Chan, S. G. Kazarian, *Macromolecules* **2004**, *37*, 6498; c) C. Xuan, Y. Zhou, Y. Zhao, X. He, L. Jin, *Phys. Rev. Appl.* **2022**, *17*, 014007; d) K. Yu, A. Xin, Q. Wang, *J. Mech. Phys. Solids* **2018**, *121*, 409; e) A. Pena-Francesch, H. Jung, M. C. Demirel, M. Sitti, *Nat. Mater.* **2020**, *19*, 1230.

© 2023 The Authors. Advanced Materials published by Wiley-VCH GmbH

15214095, 2023, 22, Downloaded from https://onlinelibrary.wiley.com/doi/10.1002/adma.202211763 by Michigan State University, Wiley Online Library on [28/09/2023]. See the Terms and Conditions (https://onlinelibrary.wiley.com/terms-and-conditions) on Wiley Online Library for rules of use; OA articles are governed by the applicable Creative Commons License